scientific reports

OPEN

Computational investigation on the hydrodynamic performance of a vertically submerged plate-type wave energy converter under variable relative openings

Surendra Singh Yadav[1], Sujit Roy[2] & Pushpendra Kumar Singh Rathore[3]✉

This study aspires to analyze a wave energy converter (WEC) through its hydrodynamic efficiency featuring a stationary submerged thin vertical plate (STVP) situated at free surface level ($z = 0$ m). The investigation incorporates arrangements with both flat and uneven seabed profiles, and also various wave steepness conditions. To perform the computational work, a numerical wave tank (NWT) is developed utilizing the ANSYS Fluent 2024 R2 software, and the fluid interface tracking is done employing the volume of fluid (VOF) approach. Stokes waves of second-order are produced at NWT entrance using the inflow velocity approach, and the wave reflection is minimized at the end by using numerical damping. The effect of four distinct relative opening (α) and wave height (H), with uneven bottom, is evaluated and subsequently compared to the hydrodynamic efficiency over a flat sea bed. The study is conducted for four distinct wave time periods (T) in the range of 1.16–2 s. The axial flow velocity under the stationary plate is computed for various conditions, such as (a) thin plate only, (b) thin plate and a trapezoidal structure of distinct altitude below it. This research study illustrates that optimal efficiency occurs at $\alpha_2 = 50\%$. Additionally, axial flow velocity (v_x) exhibits elevated values at $T = 1.87$s for increased wave steepness. The findings indicate noticeably improved hydrodynamic efficiency with higher wave steepness.

Keywords Hydrodynamic efficiency, Submerged vertically thin plate, CFD, Relative opening variable topology, Second-order stokes wave

List of Symbols

d	Depth of water
g	Gravitational acceleration
H	Incoming wave height
a	Wave amplitude
T	Time period
P_{flow}	Water flow power
α_q	Volume fraction function
ρ	Density
φ	Velocity potential
α	Relative opening
ω	Angular frequency
L	Wavelength
k	Wavenumber
p	Pressure
V	Velocity
t	Time

[1]Department of Mechanical Engineering, Guru Nanak Dev University, Amritsar 143005, Punjab, India. [2]University Centre for Research and Development, Chandigarh University, Mohali 140301, Punjab, India. [3]Department of Mechanical Engineering, Manipal University Jaipur, Jaipur 303007, Rajasthan, India. ✉email: pushpendra.rathore@jaipur.manipal.edu

P_{wave} Wave power
x Distance from the inlet boundary in x-direction
μ Viscosity
η Surface elevation
h Height of opening
b Width of opening area beneath the plate

Abbreviations

BC Boundary Condition
CFD Computational Fluid Dynamics
GE Governing Equation
NWT Numerical Wave Tank
OWC Oscillating Water Column
SD Submergence Depth
STVP Submerged Thin Vertical Plate
VOF Volume of Fluid
WEC Wave Energy Converter

Several countries have pledged to minimize carbon dioxide emissions and become carbon-neutral to combat climate change. To achieve this goal, new energy sources must be promoted as a replacement for fossil fuels. Among the available clean energy technologies, sea waves are notable for having exceptional energy density. This attribute emphasizes the substantial potential inherent in harnessing wave energy, positioning it as a formidable contender among sustainable energy alternatives[1]. To harness this abundant energy from the ocean, diverse wave energy converters (WECs) are currently under development. These encompass a variety of designs like Oscillating Water Column (OWC)[2], bottom-hinged pitching devices[3], floating pitching devices[4], and point absorbers[5,6]. Among these, OWC type WEC is largely investigated by the researcher.

Wang et al.[7] integrated horizontal bottom plate within a two-chamber OWC to extract the wave energy more efficiently. They noticed that the presence of bottom plate has enhanced the extraction of wave power from the front chamber, whereas it affects negatively in back chamber. They found optimal length of bottom plate to be 1.5 times of dual-chamber combined width. Ko and Tsai[8] developed a novel perforated OWC to extract wave energy more efficiently and found the optimum porosity of perforation to be 0.5. They also explored dependency of hydrodynamic efficiency on the underwater opening height and identified 0.6 as the optimum opening. Lin et al.[9] implemented a geometric modification to the OWC front chamber wall by incorporating a sawtooth profile and found that the alteration is able to suppress large-scale vortex formation. Due to a decrease in hydrodynamic resistance, the wave energy conversion was enhanced by 10–25%. Gaspar et al.[10] altered the water column wall with a wall slope of 40° and compared that with the conventional OWC. They found that the modified wall has higher hydrodynamic efficiency, whereas the efficiency fluctuation due to change in wave period is less in the conventional one. Qu et al.[11] introduced an elliptical modification to the OWC rectangular front wall and found as much as 25% enhancement in wave energy conversion efficiency. Mandev and Altunkaynak[12] altered OWC front chamber wall with a cylindrical structure, which is able to minimize the separation of flow at the entrance to the chamber. They observed that the modification has improved the capture width ratio, inversely proportional to the cylinder diameter. The maximum wave forces on a truncated cylinder were experimentally and numerically inspected by Fan et al.[13]. The effects of incident wave characteristics and submergence depth (*SD*) on the magnitude of maximum wave-induced forces and associated transfer function responses were systematically analyzed. The wave force's horizontal component varied proportionally to wave steepness (H/L) but remained stable at $SD = 0.104$, whereas, vertical force steadily decreased with increasing H/L. The wave components (vertical and horizontal) remained unchanged at $SD = 0.053$ and 0.104, but at $SD = 0$, the horizontal component increased owing to wave-induced impulsive loading on the lower face of the cylinder. The linear component of vertical force decreased with deeper submergence. So far, plate type WEC is not widely recognized by the researchers. In order to create a novel form of the WEC, it is thus required to study the efficiency and wave characteristics at the locality of a vertically immersed thin plate. The wave-structure interaction in ocean wave flow across flat and uneven bottom conditions is analyzed numerically. With the advancement of CFD applications, cost-effective and reasonably quick analysis are now possible.

Some scholars have conducted both numerical modeling and physical experimentation on rectangular plates, elliptical plates, and cylinders. The computational studies related to wave characteristics are performed using NWT rather than physical wave tank since it is a preferred alternative to physical modelling and allows for the investigation of a wide range of wave varieties[14–16]. The impact of the surface profile on rectangular cylinders oriented parallel in the flow was investigated by[17]. Using ANSYS Fluent, Yadav and Roy[18] conducted a numerical analysis of the stability of linear waves in shallow water. Arslan et al.[19] measured the drag force and noticed the considerable eddy dynamics influence on flow behavior around a partially submerged rectangular cylinder. Roy and Ghosh[20] utilized the Morison relationship[21] for computing wave forces acting upon a 2-D submerged thin vertical plate (STVP) at different *SD* in low-depth water. Rajagopalan and Niehous[22] explored the force value on plates using an NWT, contributing to the advancement of numerical methods for studying wave-structure interactions. Fernando and Rival[23] experimentally studied the impact of aspect ratio on plates in elliptical shape. At various submergence depths, Satheesh and Huera-Huarte[24] analyzed drag characteristics of the vertical plate with varying aspect ratios. Prasad et al.[25] simulated wave characteristics through numerical and experimental research conducted within a three-dimensional NWT. Wong et al.[26] studied flows in a distribution chamber experimentally and numerically. A 2-D and 3-D model were compared to explore the flow in the chamber.

Patten[27] highlighted future trends in offshore engineering and other marine resources in the order of renewable energy. Furthermore, Lynos[28] summarized the advancements in offshore technology and field developments. Many countries recognize wave energy from ocean as a significant and promising energy source. Wave energy obtained from the ocean is a renewable source of energy, but there has been very little technological progress in this area compared to other sources of energy[29]. Wang and Zhang[30] investigated a submerged horizontal plate connected offshore OWC in terms of its hydrodynamic efficiency. Elhanafi et al.[31] conducted a computational hydrodynamic analysis of an offshore OWC using CFD. The efficiency is influenced by wave amplitude, according to Luo et al.[32]. Furthermore, Ning et al.[33]– [34] investigate numerically and experimentally hydrodynamic efficiency and show that as wave amplitude rises, efficiency increases and eventually drops. Dong et al.[35]– [36] calculated the wave force on an immersed horizontal plate over variable topography. Qiao et al.[37] considered the impact of porosity and wave characteristics on wave force using computational and experimental approaches. Orer and Ozdamar[38] performed experimental research to explore the energy efficiency of a submerged horizontal plate WEC under three different bottom conditions below the plate. Sangtarash and Roohi[39] used OpenFOAM software to quantitatively study nonlinear wave interaction with a particular WEC. Chappelear[40] presented the first numerical method and advanced by Dean[41] centered on the stream function theory. Inviscid and irrotational flow are the assumptions behind these numerical techniques.

Novelty and objective of the present study
According to the above literature review, the flow behavior around the stationary STVP WEC under the varying relative opening and geometrical arrangement is not widely recognized. Since the depth of the ocean is variable due to different coral reef systems and the variable topography of the seabed, it is important to consider the impact of irregular bottom conditions on WEC performance. As of now, research on the hydrodynamic energy of waves has not included an investigation of how waves interact with an STVP-type WEC under uneven seabed circumstances. This particular aspect remains unexplored, highlighting a gap in current research that underscores the need for comprehensive examinations of the WECs performance under varying seabed profiles. This research endeavor explores the effects of waves on STVP wave energy converters (WECs) with varying topologies. Additionally, it examines how the relative opening affects the hydrodynamic efficiency of the STVP WEC across distinct wave steepness conditions. By taking into account the advancement of WEC in the surge direction, this research presents a novel viewpoint for researchers to consider.

Practical application of the present study
Figure 1 demonstrates how the findings of the present study can be applied in a real-world scenario. The proposed STVP WEC shows strong potential for extracting renewable energy from ocean waves through enhanced hydrodynamic performance. Acting as a hydrodynamic energy modulator, the STVP converts incident wave energy into localized flow acceleration and pressure gradients. As waves interact with the submerged plate, diffraction and partial reflection produce a downstream pressure drop, which accelerates flow beneath and around the plate. This generates a high-velocity wake that increases the available kinetic energy for the axial turbine. The turbine subsequently converts this accelerated flow into mechanical power, while the uneven seabed further modifies local flow patterns, reducing wave reflection and enabling more stable operation under varying wave conditions.

Numerical methodology
Governing equations (GE)
The momentum equation and the equation of continuity are expressed below to formulate the unsteady, inviscid, and incompressible flow condition[42]:

$$\frac{\partial \bar{u}_i}{\partial x_i} = 0\,(i = 1,\ 2) \tag{1}$$

$$\rho\left[\frac{\partial \bar{u}_i}{\partial t} + \bar{u}_j \frac{\partial \bar{u}_i}{\partial x_j}\right] = -\frac{\partial \bar{p}}{\partial x_i} + \frac{\partial}{\partial x_j}\left[\mu \frac{\partial \bar{u}_i}{\partial x_j} - \rho\, \overline{u_i' u_j'}\right] + \rho\, g_i \tag{2}$$

where, $\rho\, \overline{u_i' u_j'}$ is the turbulent fluctuations term. This term encapsulates the apparent stresses arising from turbulent flow, commonly known as Reynolds stresses. The subscripts i, j = 1, 2, symbolize 2-D Cartesian coordinates, whereas, $\overline{p}$ and $\overline{u_i}$ denotes average pressure and average velocity, respectively.

To model the turbulent flow, RNG $k-\epsilon$ model is used, as illustrated in Eqs. (3) and (4).

$$\frac{\partial}{\partial t}(\rho\, k) + \frac{\partial}{\partial x_i}(\rho\, k u_i) = -\frac{\partial}{\partial x_j}\left[\alpha_k\, \mu_{eff} \frac{\partial k}{\partial x_j}\right] + G_k + \rho\, \epsilon \tag{3}$$

$$\frac{\partial}{\partial t}(\rho\, \epsilon) + \frac{\partial}{\partial x_i}(\rho\, \epsilon\, u_i) = -\frac{\partial}{\partial x_j}\left[\alpha_\epsilon\, \mu_{eff} \frac{\partial \epsilon}{\partial x_j}\right] + C_{1\epsilon} \frac{\epsilon}{k} G_k - C_{2\epsilon}\, \rho \frac{\epsilon^2}{k} \tag{4}$$

where, k = turbulent kinetic energy, ϵ = dissipation rate of k, G_k = production of k, μ_{eff} = diffusion coefficient, and $C_{1\epsilon}$ =1.42 & $C_{2\epsilon}$ =1.68 are the empirical constants.

The volume of fluid (VOF) method is utilized for capturing multi-phase (air-water) phenomena in NWT[43]. The volume fraction function (α_q) represents the relationship between the volume occupied by the q^{th} phase in a cell and the overall volume of the cell. This implies that if α_q = 1, the total volume of cell is full of water; if α_q = 0, the total volume of cell is air and in the remaining cases, when α_q is partially filled with water and air ($0 < \alpha_q < 1$),

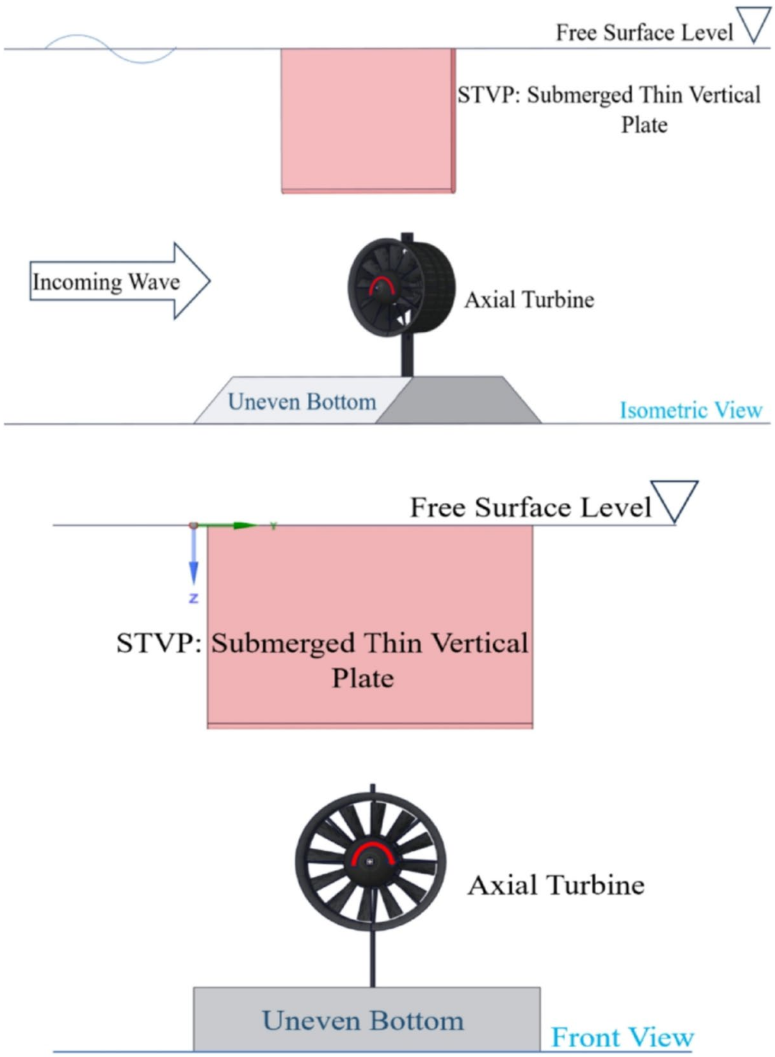

Fig. 1. Configuration of an Axial Turbine–based STVP WEC system over an uneven seabed. (Real Application)

the cell is within the water-air interface. The equations are used to calculate the properties of fluid by weighting them according to volume fraction, shown as follow:

$$\frac{\partial \alpha_q}{\partial t} + \nabla \cdot \left(\alpha_q \overline{V}\right) = 0 \quad (5)$$

$$\sum_{q=1}^{2} \alpha_q = 1 \quad (6)$$

where, $\bar{V}$ is the velocity vector. Based on the volume fraction, the two-phase mixture density is computed as follows:

$$\rho = \alpha_q \rho_w + (1 - \alpha_q)\rho_a \quad (7)$$

where, $\rho_w = 998.2$ kg/m^3 and $\rho_a = 1.225$ kg/m^3, are the density of water and air, respectively.

The hydrodynamic efficiency of the STVP WEC is calculated using following relationship:

$$Efficiency = \frac{P_{flow}}{P_{wave}} \quad (8)$$

The equations for P_{wave} and P_{flow} are as follows:

$$P_{wave} = \frac{1}{16}\rho\, gH^2 \frac{L}{T} b \left[1 + \frac{\frac{4\pi\, d}{L}}{sinh\left(\frac{4\pi\, d}{L}\right)}\right] \tag{9}$$

$$P_{flow} = \frac{1}{2}\rho\, bhv_x^3 \tag{10}$$

where, $v_{x=}$ axial velocity of wave (m/s), b=width of opening area under plate (m).

The ratio of the opening height (h) under the stationary vertical plate to the NWT's water depth (d) is known as the relative opening (α), and is mathematically shown as:

$$\alpha\ = h/d \tag{11}$$

Numerical model details

An analysis using numerical methods has been conducted to examine the 2-D rectangular domain as NWT. ANSYS Fluent 2024 R2 (ANSYS, Inc., https://www.ansys.com) CFD software is used to perform the simulation work. Figure 2 depicts the design of the 2-D NWT ($lx \times lz$), featuring (a) a flat seabed and (b) an uneven seabed within the computational domain. The domain is divided into two parts, where the upper part is filled with atmospheric air (assumed as incompressible) and the bottom part is considered as seawater. Properties of air and water are chosen based on the available material database in Fluent. The waves in the NWT are created employing an inflow approach at the inlet boundary. An open pressure vent is provided at the NWT's upper wall. A no-slip boundary constraint is applied to bottom and right solid walls. This condition ensures that the fluid velocity to be zero at the proximity of solid wall. Based on the analysis of wave stability in NWT, the numerical domain has been split into three sections: (1) wave generating zone (l_{x1} = 2 m), (2) working zone (l_{x2} = 6 m), and (3) numerical damping zone (l_{x3} = 2 m). The NWT has dimensions of l_x = 10 m and l_z = 1 m. A 2nd order Stokes waves with four distinct time periods are produced in the current study by the inflow technique. A numerical beach is implemented as a damping zone at the end of the working area toward the end wall to prevent wave reflection from the end wall of the NWT. Without this measure, waves would bounce off the end wall, causing simulation complications. The detailed geometric parameters of NWT are mentioned in Table 1. Different wave heights are considered in the present study to capture the effect of wave characteristics on the performance of WEC. The wave parameters considered in the present simulation are mentioned in Table 2.

Grid generation and grid independent test

In the present study, to discretize the 2-D computational domain, structured cells are considered (Fig. 3). Mesh refinement is adopted near the free surface level and vicinity of the plate to capture the fluid behaviour precisely. In the damping region, the element size increases gradually along the tank length until the end wall of the NWT[32]. For discretization, 1st order implicit and 2nd order upwind schemes are chosen. The Courant value is set to 0.25 to improve numerical stability and confirm the travelling information from each computational

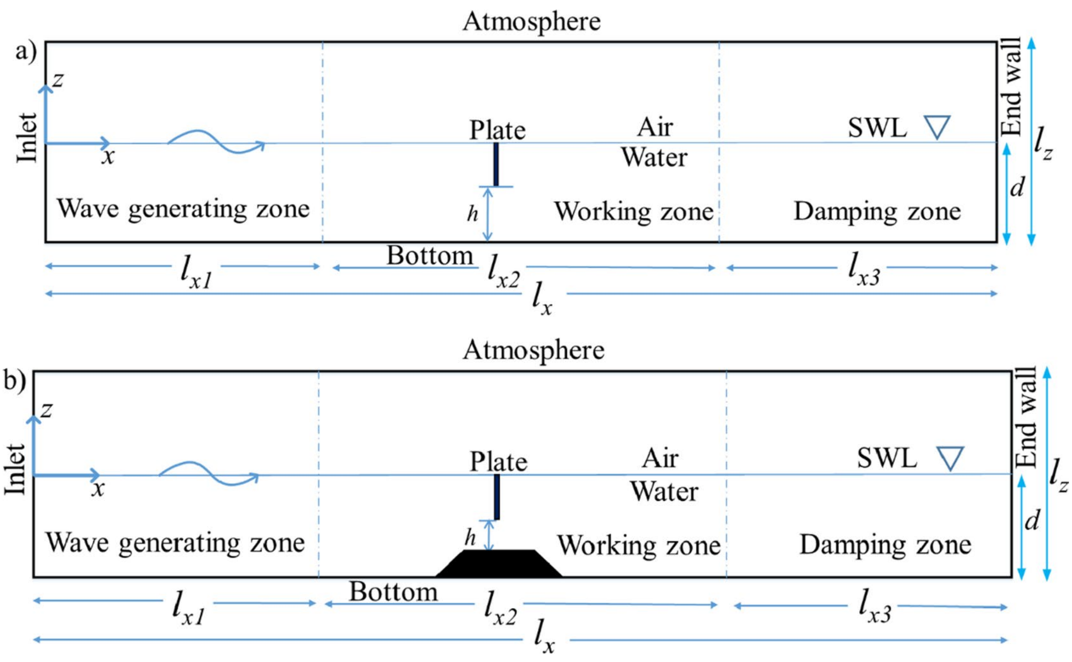

Fig. 2. Schematic of 2-D numerical wave tank **(a)** with flat seabed and **(b)** with uneven seabed in the numerical domain.

Relative opening (α)	(Flat bottom) $\alpha_1 = 62.5\%$	(Case 1) $\alpha_2 = 50\%$	(Case 2) $\alpha_3 = 43.75\%$	(Case 3) $\alpha_4 = 37.5\%$
Vertical plate height	0.15 m	0.15 m	0.15 m	0.15 m
Water depth (d)	0.4 m	0.4 m	0.4 m	0.4 m
Height of NWT (l_z) (air domain + water domain)	1 m	1 m	1 m	1 m
Wave generating zone (l_{x1})	2 m	2 m	2 m	2 m
Working zone (l_{x2})	6 m	6 m	6 m	6 m
Numerical damping zone (l_{x3})	2 m	2 m	2 m	2 m

Table 1. Geometrical parameters used in this study.

Time Period T (s)	Wave height H (m)	Wave steepness (H/L)	Water depth d (m)
1.16	0.04	0.0217	0.4
1.50	0.045	0.0152	0.4
1.87	0.05	0.0117	0.4
2	0.055	0.0108	0.4

Table 2. Wave parameters considered in the present study.

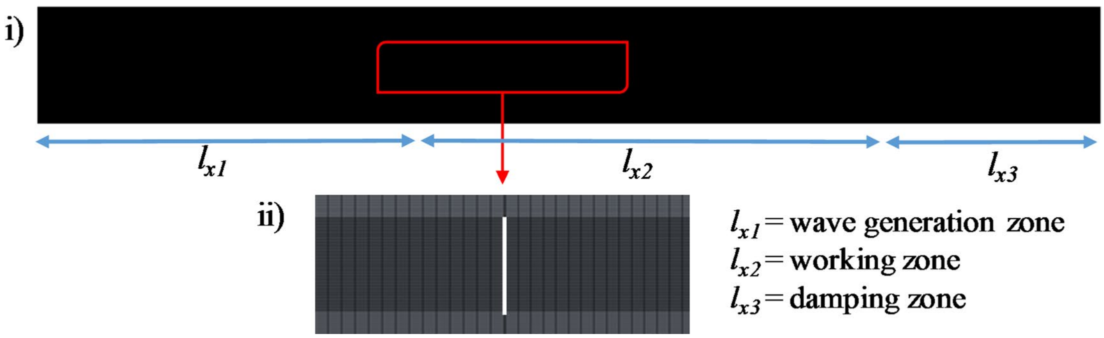

Fig. 3. (***i***) Structured grid of 2-D NWT and (***ii***) zoomed view near the vertical plate.

	Mesh 1	Mesh 2	Mesh 3	Mesh 4
Δx [m]	**0.03587**	**0.02562**	**0.01830**	**0.01307**
Δz [m]	0.00355	0.00253	0.00181	0.00129
No. of Elements	140,000	202,500	250,000	299,750

Table 3. Four sets of mesh Parameters.

sub-domain. The numerical model is simulated with 5000-time steps (time-step size = 0.01s), with a maximum iteration of 20. The convergence criteria are set to 10^{-6} for all the governing equations.

Optimizing the mesh size is essential since it reduces computing effort. Therefore, the grid independence test is performed to detect independence from the grid system utilized for this research study. Four systematically refined meshes are generated by reducing the grid spacing in both directions by a factor of approximately 1.4. The detailed mesh parameters are mentioned in Table 3. The test is carried out considering surface profile at $x = 4.5$ m for wave height $H = 0.05$ m and period $T = 1.1658$s at free surface $z = 0$ m for four different mesh conditions. In Fig. 4, the surface elevation results obtained from two different meshes, namely mesh 3 and mesh 4, are being compared. Mesh 3 and mesh 4 yield similar results in terms of surface elevation, with a difference of 0.0005% between their numerical results. Therefore, the grid size of mesh 3 is sufficient to achieve accuracy, and mesh 3 is adopted for further simulation.

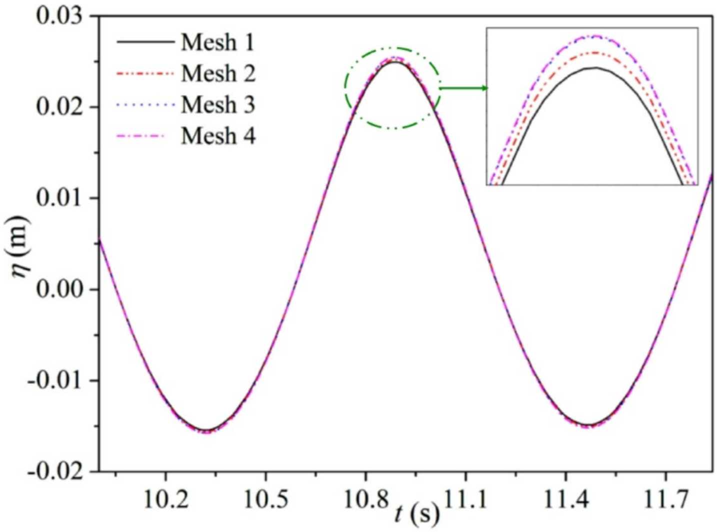

Fig. 4. Surface elevation at $x = 4.5$ m for different grids.

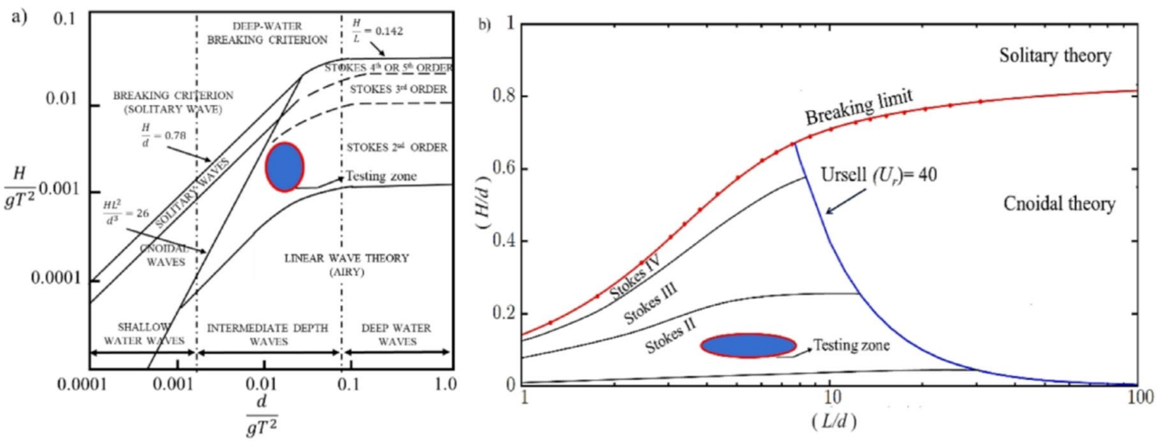

Fig. 5. Limit of application of various wave theory based on **(a)** Le Mehaute[46], **(b)** Fenton[47].

Wave theory validation

The validation zones of different wave theories are represented in Fig. 5. The applicability of various theories is influenced by water depth (*d*), wavelength (*L*), and wave height (*H*). The Ursell number (*Ur*), according to Fritz Ursell, is the ratio of nonlinearity (*H/d*) to shallowness (d^2/L^2). The *Ur* is the criterion for separating the boundary between Stokes wave theories and cnoidal wave theories[44]. As shown in Fig. 5, the wave parameter employed in this numerical analysis is in the second order Stokes zone (Testing Zone). Ensuring the accuracy of our present numerical technique is imperative before commencing the main investigation. A validation test has been executed to assess the correctness of the numerical study. The time-dependent surface elevation (η) is displayed at $x = 0.55$ m to validate the solver. The outcomes generated by the current model are matched with the experimental and numerical data previously published by Gao[45], as illustrated in Fig. 6. The close alignment with the reference[45] serves as a testament to the correctness and reliability of the current CFD model.

Results and discussion

The current investigation focused on the performance of a stationary STVP WEC in NWT under intermediate water depth. An NWT model is created in the ANSYS Fluent 2024 R2 (ANSYS, Inc., https://www.ansys.com) CFD software. Various structural heights of the uneven bottom structure have been taken to assess the impact of uneven bottom conditions on the wave flow below the stationary vertical rectangular thin plate. Since the depth of the ocean varies due to different coral reef systems and the variable topography of the seabed, it is crucial to consider the impact of irregular seabed conditions on wave flow and the hydrodynamic performance of WEC. To investigate the impact of variable topography in a study of wave-body interaction, three distinct heights of uneven bottom structures are introduced. This study has been performed for *T* (wave time periods) 1.16, 1.50,

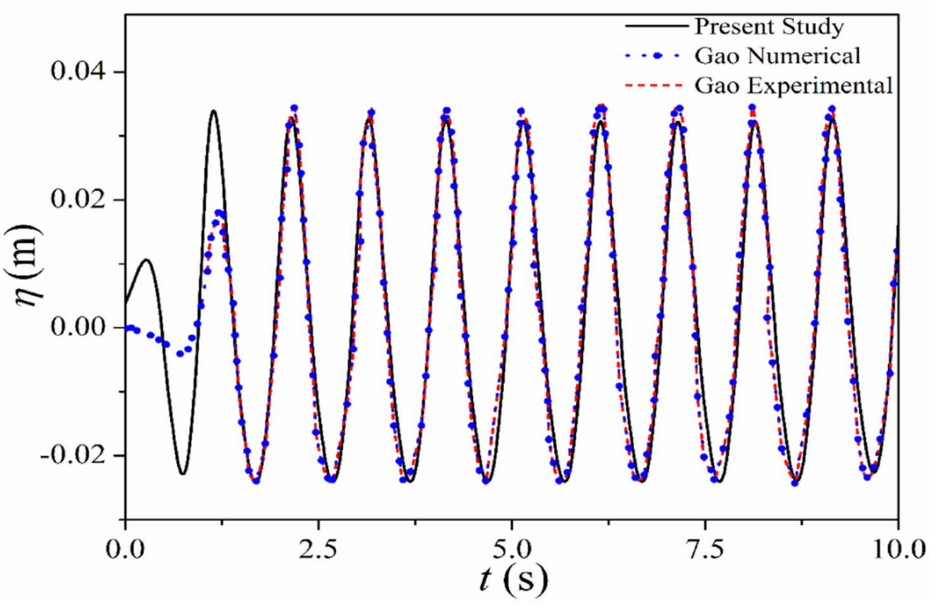

Fig. 6. Validation of the present computational model with results of Gao[45] in terms of surface elevation (η).

1.87, and 2s and H (wave heights) 0.04, 0.045, 0.05, and 0.055 m. The effects of relative opening with and without a vertical plate on the axial flow velocity, velocity distribution around the opening, water-air volume fraction, and maximum hydrodynamic efficiency are studied exclusively.

Effect on axial flow velocity

Figures 7, 8, 9, 10 show the comparative representation of axial flow velocity (v_x) for different wave heights over flat and uneven bottom conditions. The influence of uneven bottom and wave parameters on axial flow velocity (v_x) has been noticed below the vertical thin plate and at a distance of $x = 4.2$ m from the inlet of the NWT. As shown in Fig. 7, for $H = 0.04$ m, the axial flow velocity component (v_x) is highest in Case 3 and exceeds that of the others at a wave period of $T = 1.87$s. This observation proved that non-linear wave attained the maximum axial flow velocity (v_x) below the plate for $H = 0.05$ m. The axial flow velocity (v_x) increases with increasing time period for all wave heights, but follows a negative trend at the highest time period, $T = 2$s. It indicates dominant wave energy dispersion at higher time period, decreasing near-plate momentum transfer. Therefore, it is noticed that axial flow velocity (v_x) depends on the wave height, slope, and height of the bottom structure. The graph of axial flow velocity (v_x) presents a periodic nature. The kinetic energy of propagating waves is greatest at $z = 0$ m (free surface) and decreases towards the bottom of the NWT. The bottom kinetic energy of propagating waves, on the other hand, is redirected by introducing an uneven bottom of appropriate size and shape. The axial flow velocity (v_x) is notably greater under uneven bottom conditions compared to a flat bottom. Similarly, in Fig. 8–10, for $H = 0.045$, 0.05, and 0.055 m, axial flow velocity (v_x) are higher for Case 3 compared to other cases. The axial flow velocity (v_x) beneath the plate from the wave maker exhibits a notable increase as the incoming wave height rises. The dominance of Case 3 indicates better wave-structure interaction and higher momentum transfer below the vertical plate. The relative opening is a critical geometrical parameter that affects the efficiency of the WEC system. Figure 11 represents the variation of maximum axial velocity with time periods. The maximum axial velocity follows a positive trend till $T = 1.87$s and attained a maximum value of 0.297 m/s for Case 3 and $H = 0.055$ m. Compared to the flat bottom, a 14.6% higher velocity is achieved with Case 3. It implies that the alterations in the seabed topography increase local acceleration of water, and it is maximum under higher wave height condition.

Effect on velocity vector distribution

The velocity-vector fields presented in Fig. 12 reveal a distinct difference in the hydrodynamic behavior between the flat-bottom configuration and the modified seabed layout (Case 1) in STVP Configuration. As all the modified seabed cases following same trend in momentum transfer, Case 1 is selected for the comparison. In the flat-bottom case, the incoming flow remains relatively uniform with weak, scattered vortical structures throughout the simulation, indicating limited wave–structure interaction. In contrast, Case 1 demonstrates a clear intensification of flow dynamics. Between time-steps, $t = 2$–3 s, a well-defined recirculation cell develops near the seabed opening, accompanied by elevated velocity gradients concentrated along the lower portion of the thin submerged vertical plate. This indicates that the opening effectively redirects and channels the incoming wave energy beneath the STVP. As the simulation progresses to $t = 4$–7 s, the flat-bottom case continues to exhibit mild shear and weak recirculation that does not significantly influence energy transport. However, Case 1 shows the emergence of a strong downstream vortex that increases in strength and spatial extent, along with high-velocity jets near the plate tip and at the outlet of the seabed opening. By $t = 8$–10 s, multiple large

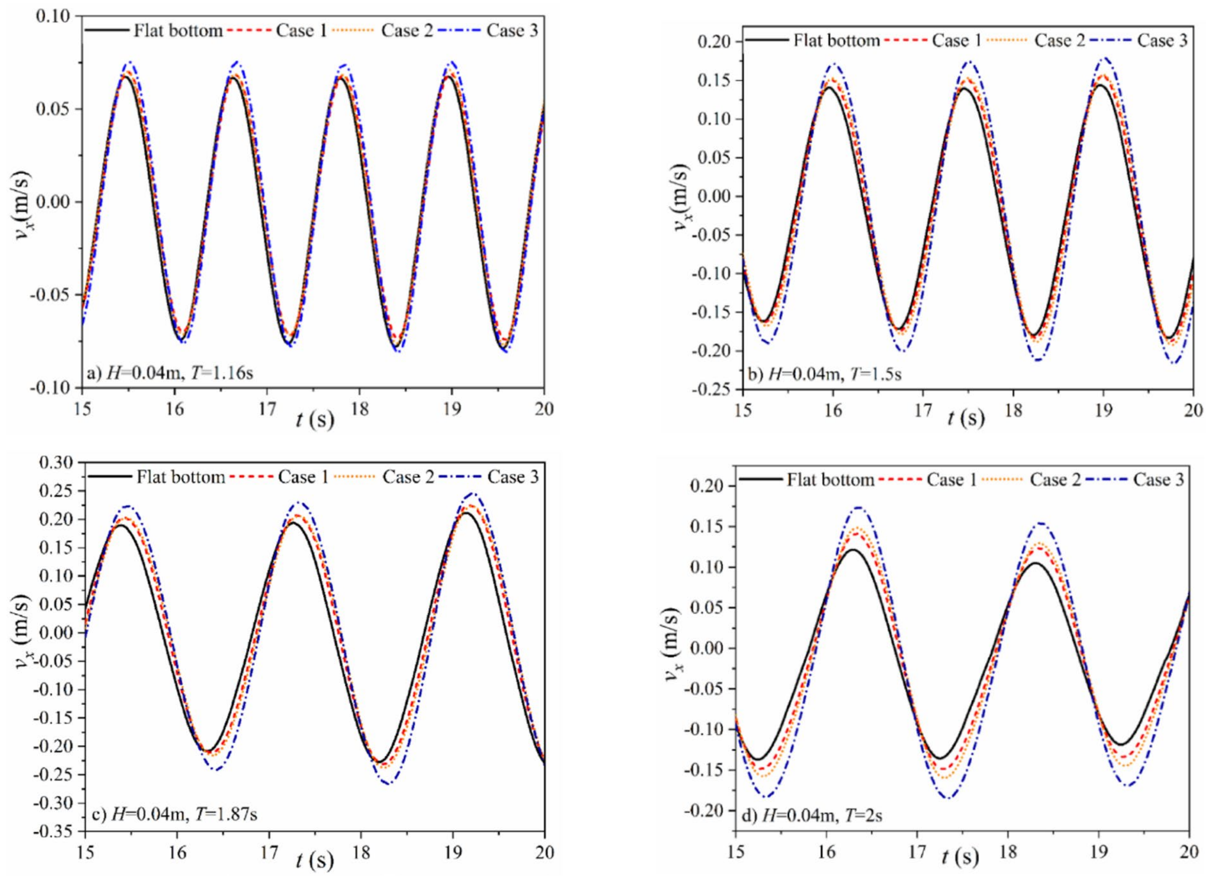

Fig. 7. Comparison of axial flow velocity (v_x) for different time period over flat and uneven bottom conditions at $x=4.2$ m below the vertical plate for $H=0.04$ m.

and coherent vortices dominate the interaction zone, and the velocity field reaches its maximum intensities, particularly below and behind the plate. These persistent, high-energy rotational structures demonstrate that the seabed opening effectively traps, accelerates, and redirects wave-induced momentum beneath the plate, thereby enhancing hydrodynamic loading and oscillatory response. This localized concentration of kinetic energy significantly improves the energy-capture potential of the system. For axial-turbine-based STVP configurations WEC, the increased near-plate velocities and strengthened vortices directly translate to higher excitation forces and improved power extraction. Importantly, this hydrodynamic enhancement is achieved passively through seabed geometry modification alone, offering a practical and cost-efficient strategy to increase overall WEC performance without altering the device structure.

Effect on wave propagation

The phase diagrams shown in Fig. 13 further confirm the influence of the seabed opening on wave–structure interaction. For the flat-bottom condition, the free surface remains nearly linear with minimal disturbance near the plate, indicating weak coupling between the incident wave and the STVP. In Case 1, however, a distinct upward displacement of the free surface develops near the plate from $t=3$–5 s, caused by localized wave focusing and pressure amplification induced by the seabed geometry. This elevated interface demonstrates that the modified bathymetry increases wave momentum transfer into the interaction zone. Such free-surface amplification is beneficial in real WEC deployments because it enhances the effective wave height acting on the device, enabling higher energy capture even under moderate sea states. The improved phase response, therefore, highlights the practical advantage of integrating seabed modifications to passively strengthen the energy available for conversion. Together, these hydrodynamic enhancements confirm that Case 1 offers superior efficiency compared to the flat-bottom configuration, establishing seabed-geometry optimization as a practical and effective strategy for improving real-world wave energy conversion performance.

Effect on hydrodynamic efficiency

This computational investigation analyses the performance of an STVP WEC for four distinct relative openings (α) and four wave heights (H). Figure 14 portrays the variation of hydrodynamic efficiency with time period for varied α and H at $d=0.4$ m. Consequently, the efficiency of the WEC augments with the escalation of wave heights. The plate itself, without any structure forms below (flat bottom), has a maximum efficiency of 25.73% for wave height $H=0.04$ m and relative opening $\alpha_1=62.5\%$. Further, the effect of relative opening is analysed

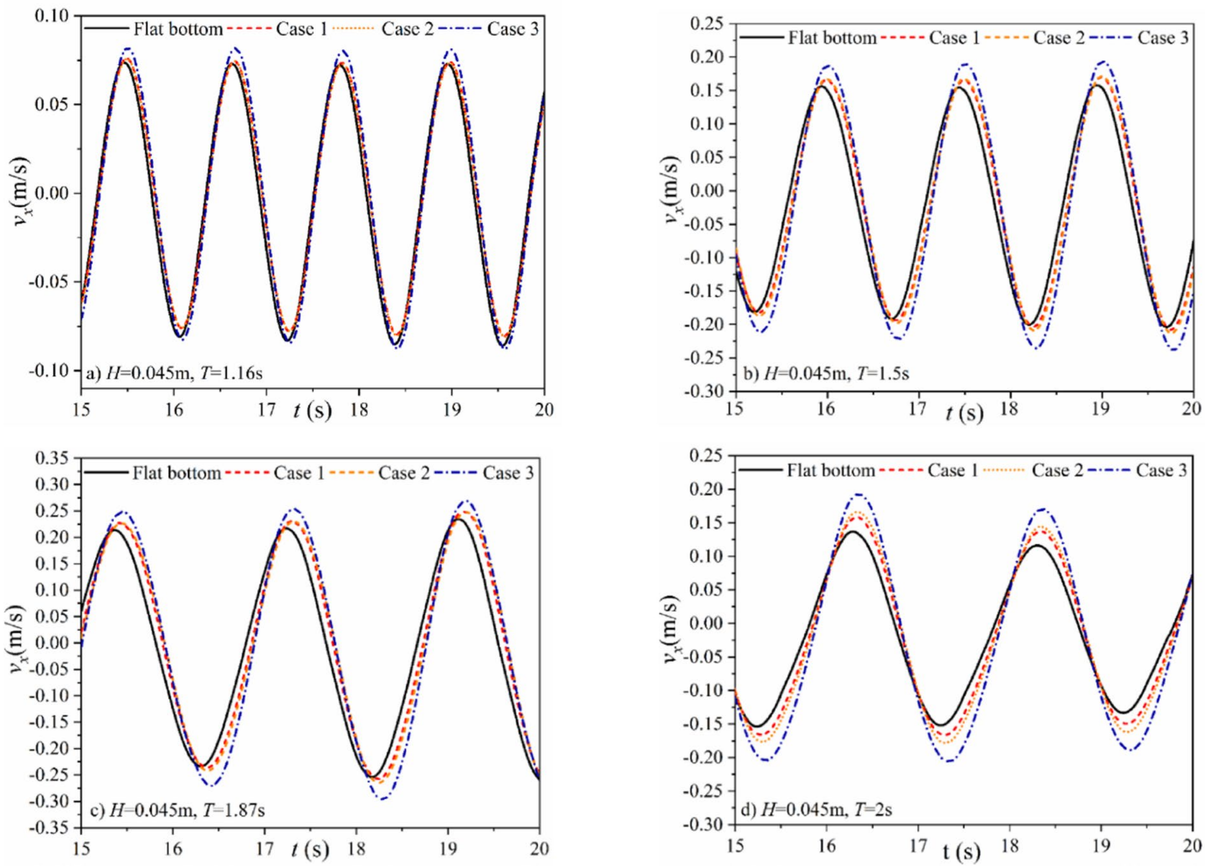

Fig. 8. Comparison of axial flow velocity (v_x) for different time period over flat and uneven bottom conditions at $x = 4.2$ m below the vertical plate for $H = 0.045$ m.

with different incoming wave height conditions. The highest efficiency value, reaching 34.9%, is achieved by positioning a trapezoidal structure below the plate, with the distance between the top surface of the trapezoidal structure and the bottom of the vertical plate set to 0.2 m. This configuration corresponds to Case 1, where the relative opening α_2 is set to 50%. The efficiency value is obtained to be small for all incoming wave heights for the short time periods. The maximum value of efficiency is recorded for the time period $T = 1.87$s. For a higher time period, the magnitude of efficiency is low once more for all wave heights. When the efficiencies of Case 1, Case 2, Case 3 in which the trapezoidal form makes a passage of 0.2 m, 0.175 m, and 0.15 m below the plate where water flows are compared with flat bottom conditions, Case 1 seems to be more efficient for all wavelengths. The highest efficiency is observed in Case 1 ($\alpha_2 = 50\%$) at a time period of $T = 1.87$s for all wave heights. This suggests that a trapezoidal structure is preferable to a flat bottom. Therefore, the outcome for $H = 0.055$ m would be advantageous for practical applications. This suggests that deploying a trapezoidal structure with a relative opening $\alpha_2 = 50\%$ would be a superior choice in terms of maximizing efficiency.

Conclusion

The current study investigates the hydrodynamic efficiency of an STVP-type WEC utilizing NWT, varying the relative openings, wave parameters, and variable topology. An NWT model is generated in ANSYS software. The VOF approach is utilized to monitor and track the interface between two fluids. Nonlinear waves are generated by employing an inflow velocity approach combined with Dirichlet BC implemented in the NWT. The influence of relative opening and wave steepness (H/L) on uneven seabed on hydrodynamic efficiency was analyzed and compared with the flat bottom case. The following concluding remarks are figured out from the above research study.

- The performance of STVP WEC is dependent on H/L and α.
- The wave energy is relatively higher for the large wave height (H) with uneven bottom conditions.
- The relative opening (α_2) of 50% showed better hydrodynamic efficiency compared to other relative openings and a flat bottom.
- Axial flow velocity (v_x) shows a higher value at $T = 1.87$s for $H = 0.055$ m.
- The highest computed efficiency is reached when relative opening (α_2) is 50%, and the time period $T = 1.87$s.

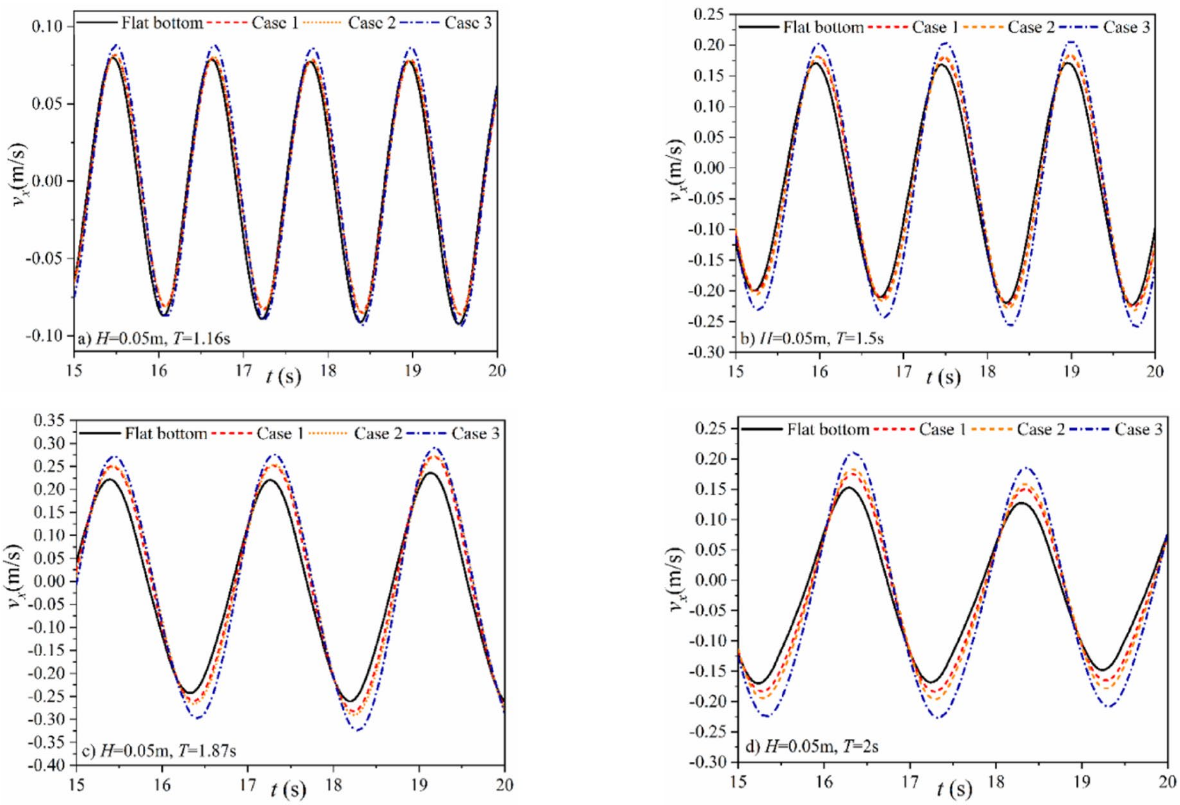

Fig. 9. Comparison of axial flow velocity (v_x) for different time period over flat and uneven bottom conditions at $x = 4.2$ m below the vertical plate for $H = 0.05$ m.

Thus, the result for $H = 0.055$ m and $T = 1.87$s would be advantageous for applications, suggesting that installing with a relative opening $\alpha_2 = 50\%$ would offer superior hydrodynamic performance. As a result, the presented STVP-type WEC can be efficiently employed for extracting wave energy with suitable dimensions. Therefore, the present research will confirm that STVP-type WEC will be more commonly employed in the future for the extraction of renewable energy.

Limitations of the present study and future scope

In the present computational study, waves were generated using standard wave height and wavelength in intermediate water depth, with validation based on the Le Mehaute[46] and Fenton graph[47], demonstrating appropriate application of wave theory. However, in real ocean conditions, wave characteristics are not constant; they are influenced by various factors such as environmental conditions and the geological features of the region.

The present study will be extended, incorporating the following aspects:

- Researchers can explore the potential of WECs in shallow and deep-water conditions with varying wave characteristics, tailored to specific application scenarios.
- Given the uneven nature of the ocean bed, future studies can further investigate the impact of seabed topography other than trapezoidal on the hydrodynamic efficiency of WECs.

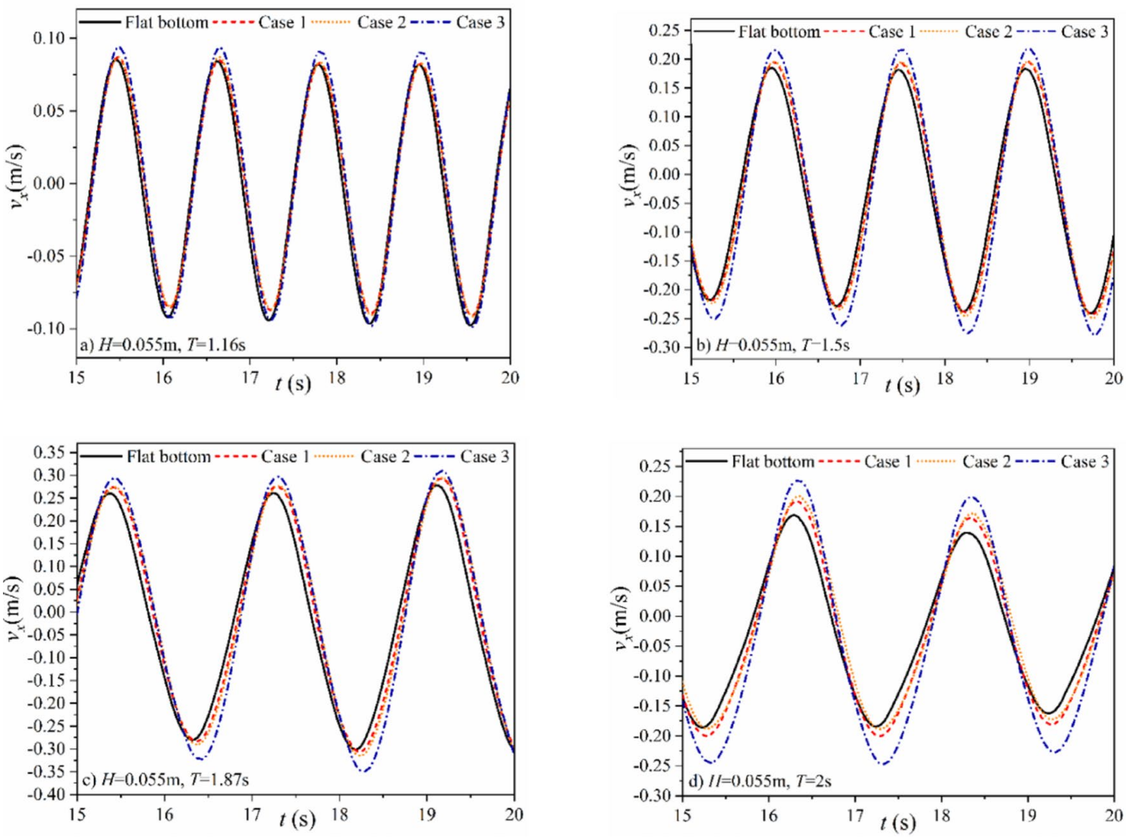

Fig. 10. Comparison of axial flow velocity (v_x) for different time period over flat and uneven bottom conditions at $x=4.2$ m below the vertical plate for $H=0.055$ m.

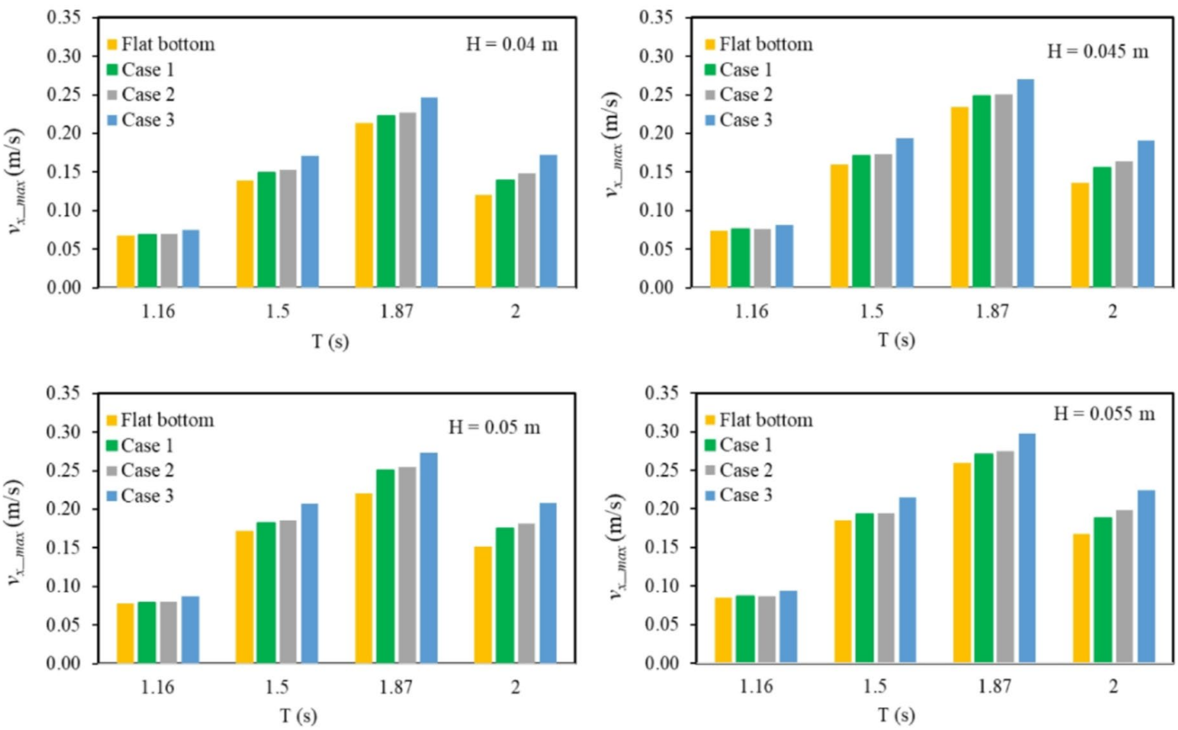

Fig. 11. Variation of maximum axial flow velocity with time period for different wave height.

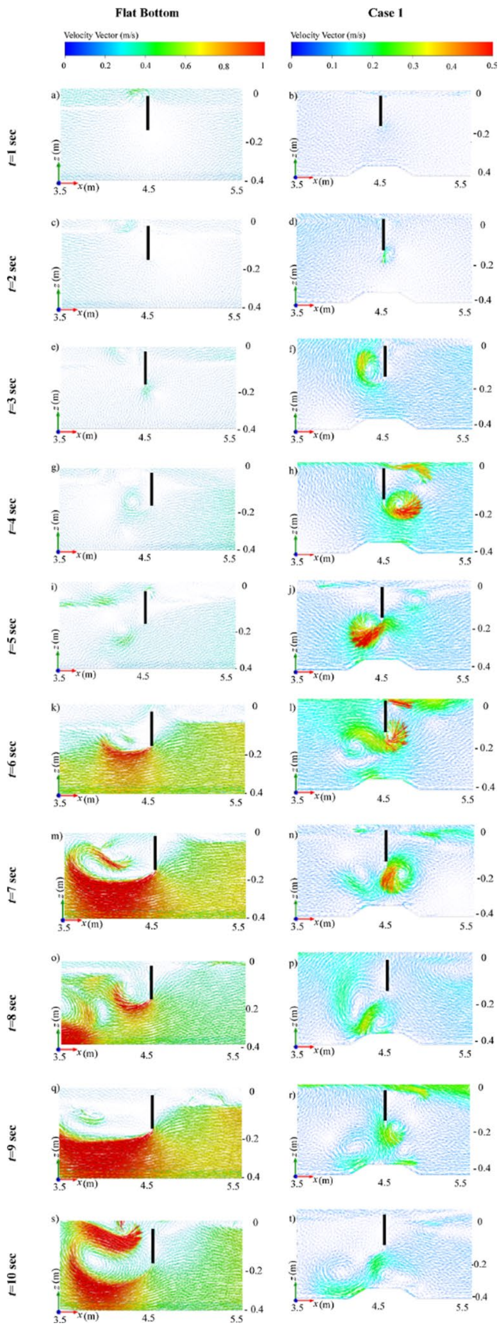

Fig. 12. Velocity vector fields at successive flow times (t) for the Flat Bottom and Case 1 configurations at $H = 0.055$ m with a wave period of $T = 2$s.

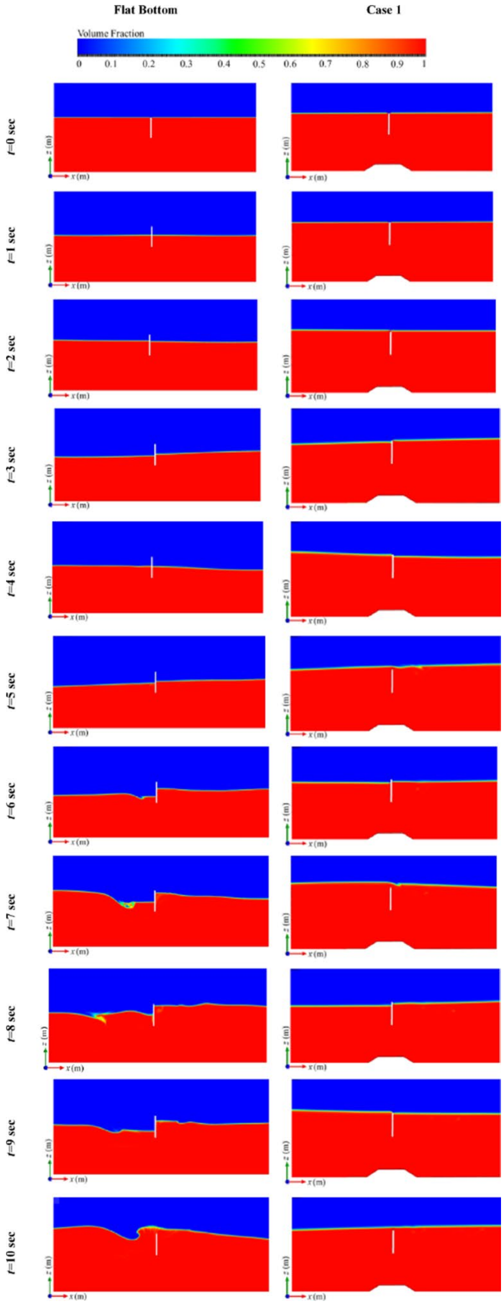

Fig. 13. Wave propagation over time for flat bottom and Case 1 at T=2 s at relative water depth d = 0.4 m.

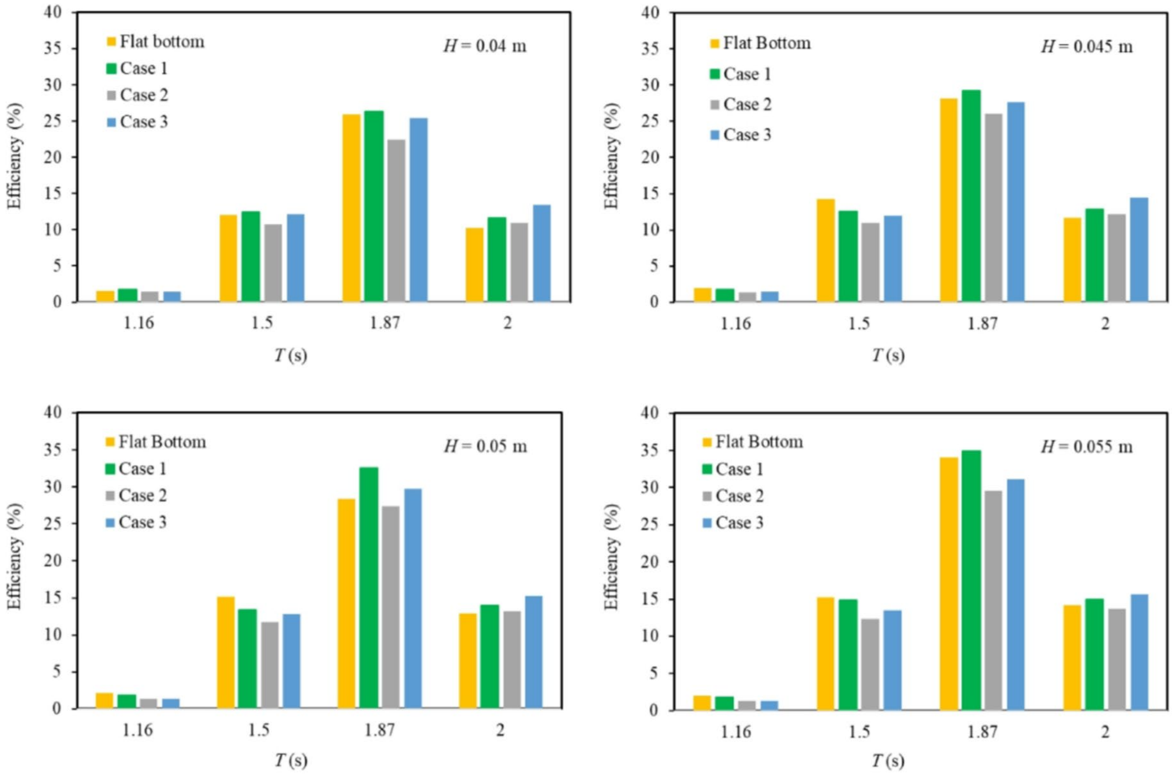

Fig. 14. Hydrodynamic efficiency versus time period (T) for different relative opening (α) at relative water depth $d=0.4$ m.

Data availability

The datasets generated during and/or analysed during the current study are available from the corresponding author on reasonable request.

Received: 1 September 2025; Accepted: 29 January 2026
Published online: 24 March 2026

References

1. Drew, B., Plummer, A. R. & Sahinkaya, M. N. *A Review of Wave Energy Converter Technology* (Sage Publications Sage UK, 2009).
2. He, F., Lin, Y., Pan, J. & Wei, M. Experimental investigation of vortex evolution around oscillating water column wave energy converter using particle image velocimetry. *Physics of Fluids*, **35**(1), 015151 (2023).
3. Senol, K. & Raessi, M. Enhancing power extraction in bottom-hinged flap-type wave energy converters through advanced power take-off techniques. *Ocean Eng.* **182**, 248–258 (2019).
4. Xu, Q. et al. Parametric analysis of a two-body floating-point absorber wave energy converter. *Physics of Fluids*, **35**(9), p.097115 (2023).
5. Fernandes, A. M. & Fonseca, N. Finite depth effects on the wave energy resource and the energy captured by a point absorber. *Ocean Eng.* **67**, 13–26 (2013).
6. Soleimani, K., Ketabdari, M. J. & Gharechae, A. Smoothed particle hydrodynamics study of a heaving point absorber in various waves using wave tank and calm-water models. *Physics of Fluids*, **35**(3), p.033116 (2023).
7. Wang, L., Xie, C., Deng, Y., Wu, Y. & Deng, Z. Numerical and experimental study on the hydrodynamic performance of an offshore-stationary dual-chamber OWC wave energy converter with a horizontal bottom-plate. *Ocean Engineering*, 310, p.118793. (2024).
8. Ko, C. H. & Tsai, C. P. Hydrodynamic performance of an OWC wave energy converter combined with a perforated wall. *Ocean Eng.* **327**, 120955 (2025).
9. Lin, Y. et al. Enhancing the efficiency of oscillating water column wave energy converters with sawtooth-shaped front walls: An experimental investigation. *Energy* (article in press) (2025).
10. Gaspar, L. A., Teixeira, P. R. & Didier, E. Numerical analysis of the performance of two onshore oscillating water column wave energy converters at different chamber wall slopes. *Ocean Eng.* **201**, 107119 (2020).
11. Qu, M., Yu, D., Xu, Z. & Gao, Z. The effect of the elliptical front wall on energy conversion performance of the offshore OWC chamber: A numerical study. *Energy* **255**, 124428 (2022).
12. Mandev, M. B. & Altunkaynak, A. Cylindrical frontwall entrance geometry optimization of an oscillating water column for utmost hydrodynamic performance. *Energy* **280**, 128147 (2023).
13. Fan, Y., Li, J., Liu, S. & Zhang, H. Experimental and numerical analysis of wave forces on a vertical truncated cylinder with different depths of submergence under focused waves. *Ocean Eng.* **309**, 118523 (2024).
14. Anbarsooz, M., Passandideh-Fard, M. & Moghiman, M. Fully nonlinear viscous wave generation in numerical wave tanks. *Ocean Eng.* **59**, 73–85 (2013).
15. Wang, R. Q., Ning, D. Z., Zhang, C. W., Zou, Q. P. & Liu, Z. Nonlinear and viscous effects on the hydrodynamic performance of a fixed OWC wave energy converter. *Coast. Eng.* **131**, 42–50 (2018).

16. Martin, D. et al. Numerical analysis and wave tank validation on the optimal design of a two-body wave energy converter. *Renew. Energy*. **145**, 632–641 (2020).
17. Malavasi, S. & Guadagnini, A. Interactions between a rectangular cylinder and a free-surface flow. *J. Fluids Struct.* **23** (8), 1137–1148 (2007).
18. Yadav, S. S. & Roy, P. D. Generation of stable linear waves in shallow water in a numerical wave tank. *J. Appl. Fluid Mech.* **15** (2), 537–549 (2022).
19. Arslan, T., Malavasi, S., Pettersen, B. & Andersson, H. I. Turbulent flow around a semi-submerged rectangular cylinder. *J. Offshore Mech. Arct. Eng.* **135** (4), 041801 (2013).
20. Roy, P. D. & Ghosh, S. Wave force on vertically submerged circular thin plate in shallow water. *Ocean Eng.* **33** (14–15), 1935–1953 (2006).
21. Morison, J. R., Johnson, J. W. & Schaaf, S. A. The force exerted by surface waves on piles. *J. Petrol. Technol.* **2** (05), 149–154 (1950).
22. Rajagopalan, K. & Nihous, G. Study of the force coefficients on plates using an open source numerical wave tank. *Ocean Eng.* **118**, 187–203 (2016).
23. Fernando, J. N. & Rival, D. E. Reynolds-number scaling of vortex pinch-off on low-aspect-ratio propulsors. *J. Fluid Mech.* **799**, R3 (2016).
24. Satheesh, S. & Huera-Huarte, F. J. Effect of free surface on a flat plate translating normal to the flow. *Ocean Eng.* **171**, 458–468 (2019).
25. Prasad, D. D., Ahmed, M. R., Lee, Y. H. & Sharma, R. N. Validation of a piston type wave-maker using numerical wave tank. *Ocean Eng.* **131**, 57–67 (2017).
26. Wong, V. H., Thompson, C. P. & Avery, P. A computational and experimental study of flows in a distribution chamber: validation of a numerical model. *Proc. Institution Mech. Eng. Part. E: J. Process. Mech. Eng.* **213** (4), 217–230 (1999).
27. Patten, T. Future trends in offshore engineering. *Proc. Institution Mech. Eng. Part. E: J. Process. Mech. Eng.* **208** (2), 97–106 (1994).
28. Lyons, G. J. Offshore technology—advances at the dawn of the new millennium reviewed from a UK perspective. *Proc. Institution Mech. Eng. Part. E: J. Process. Mech. Eng.* **214** (1), 1–21 (2000).
29. Falcão, A. F. D. O. Wave energy utilization: A review of the technologies. *Renew. Sustain. Energy Rev.* **14** (3), 899–918 (2010).
30. Wang, C. & Zhang, Y. Hydrodynamic performance of an offshore Oscillating Water Column device mounted over an immersed horizontal plate: A numerical study. *Energy* **222**, 119964 (2021).
31. Elhanafi, A., Fleming, A., Macfarlane, G. & Leong, Z. Numerical hydrodynamic analysis of an offshore stationary–floating oscillating water column–wave energy converter using CFD. *Int. J. Naval Archit. Ocean. Eng.* **9** (1), 77–99 (2017).
32. Luo, Y., Nader, J. R., Cooper, P. & Zhu, S. P. Nonlinear 2D analysis of the efficiency of fixed oscillating water column wave energy converters. *Renew. Energy*. **64**, 255–265 (2014).
33. Ning, D. Z., Shi, J., Zou, Q. P. & Teng, B. Investigation of hydrodynamic performance of an OWC (oscillating water column) wave energy device using a fully nonlinear HOBEM (higher-order boundary element method). *Energy* **83**, 177–188 (2015).
34. Ning, D. Z., Wang, R. Q., Zou, Q. P. & Teng, B. An experimental investigation of hydrodynamics of a fixed OWC wave energy converter. *Appl. Energy*. **168**, 636–648 (2016).
35. Dong, J., Xue, L., Cheng, K., Shi, J. & Zhang, C. An experimental investigation of wave forces on a submerged horizontal plate over a simple slope. *J. Mar. Sci. Eng.* **8** (7), 507 (2020).
36. Dong, J., Wang, B., Zhao, X. & Liu, H. Wave forces exerted on a submerged horizontal plate over an uneven bottom. *J. Eng. Mech.* **144** (6), 04018030 (2018).
37. Qiao, D. et al. Numerical simulation and experimental analysis of wave interaction with a porous plate. *Ocean Eng.* **218**, 108106 (2020).
38. Orer, G. & Ozdamar, A. An experimental study on the efficiency of the submerged plate wave energy converter. *Renew. Energy*. **32** (8), 1317–1327 (2007).
39. Sangtarash, A. & Roohi, E. Numerical investigation of wave interactions in an experimental wave-energy converter using OpenFOAM. *Proceedings of the Institution of Mechanical Engineers, Part A: Journal of Power and Energy*, ***235***(5), 1205–1224 (2021).
40. Chappelear, J. E. Direct numerical calculation of nonlinear ocean waves. *J. Phys. Res.* **66**, 501–508 (1961).
41. Dean, R. G. Stream function representation of nonlinear ocean waves. *J. Phys. Res.* **70** (18), 4561–4572 (1965).
42. Fluent, I. & ANSYS FLUENT 14. : Theory Guide Fluent Inc, Canonsburg, PA, USA; (2012).
43. Hirt, C. W. & Nichols, B. D. Volume of fluid (VOF) method for the dynamics of free boundaries. *J. Comput. Phys.* **39** (1), 201–225 (1981).
44. Hedges, T. S. & Ursell Regions of validity of analytical wave theories. *Proceedings of the Institution of Civil Engineers-Water Maritime and Energy*, **112**(2), 111–114. (1995).
45. Gao, F. *An efficient finite element technique for free surface flow*. Doctoral Dissertation, University of Brighton, UK. (2003).
46. Le Méhauté, B. *An Introduction To Hydrodynamics and Water Waves* (Springer Science & Business Media, 2013).
47. Fenton, J. D. Nonlinear wave theories. *Sea: Ocean. Eng. Sci.* **9** (1), 3–25 (1990).

Acknowledgements
The authors acknowledge the Computational Laboratory at Chandigarh University, Mohali, Punjab, India for providing the computational resources and support that contributed to the research results reported in this paper.

Author contributions
S.S. Yadav: Conceptualization, Methodology, Software, Validation, Formal analysis, Investigation, Visualization, Writing - original draft preparation S. Roy: Conceptualization, Supervision, Writing -review and editing P.K.S. Rathore: Supervision, Writing -review and editing.

Funding
Open access funding provided by Manipal University Jaipur.

Declarations

Competing interests
The authors declare no competing interests.

Additional information
Correspondence and requests for materials should be addressed to P.K.S.R.

Reprints and permissions information is available at www.nature.com/reprints.